Hindawi
Nanomaterials and Nanotechnology
Volume 2023, Article ID 9879371, 16 pages
https://doi.org/10.1155/2023/9879371

Research Article

Insight into the Influence of the Integrated Chitosan on the Adsorption Properties of Chitosan/Al-MCM-41 Composite for As (V) Metal Ions: Characterization and Advanced Equilibrium Studies

Mostafa R. Abukhadra,[1,2] **Fatma M. Dardir**,[3] **Ezzat A. Ahmed**,[3] **Mamdouh F. Soliman**,[3] **Sarah I. Othman**,[4] **Ahmed A. Allam**,[5] **Wail Al Zoubi**,[6] **and Mohamed S. Shaban**[7]

[1]*Geology Department, Faculty of Science, Beni-Suef University, Beni-Suef, Egypt*
[2]*Materials Technologies and their Applications Lab, Geology Department, Faculty of Science, Beni-Suef University, Beni-Suef, Egypt*
[3]*Geology Department, Faculty of Science, Assiut University, Assiut, Egypt*
[4]*Biology Department, College of Science, Princess Nourah bint Abdulrahman University, Riyadh, Saudi Arabia*
[5]*Zoology Department, Faculty of Science, Beni-Suef University, Beni-Suef, Egypt*
[6]*Materials Electrochemistry Laboratory, School of Materials Science and Engineering, Yeungnam University, Gyeongsan 38541, Republic of Korea*
[7]*Geology Department, Faculty of Science, New Valley University, Kharga, Egypt*

Correspondence should be addressed to Mostafa R. Abukhadra; abukhadra89@science.bsu.edu.eg

Received 13 May 2022; Accepted 15 November 2022; Published 9 August 2023

Academic Editor: Leander Tapfer

Ecofriendly chitosan/Al-MCM-48 (CH/Al-MCM) was synthesized from natural microcline and assessed as a potential adsorbent of As (V) ions with enhanced capacity. The As (V) adsorption properties of CH/Al-MCM were assessed in comparison with Al-MCM-41 as a single phase. The studied CH/Al-MCM exhibits 178.6 mg/g as As (V) adsorption capacity which is higher than Al-MCM-41 (124 mg/g). The adsorption properties were illustrated based on the pseudo-first-order kinetic, Langmuir isotherm, and monolayer model with one energy site. Based on the recognized steric parameters, CH/Al-MCM displays significant enhancement in the active sites density (Nm = 88.8 mg/g (20°C)) as compared to Al-MCM (Nm = 61.5 mg/g). This signifies the role of the chitosan integration process in enhancing the adsorption capacity by increasing the availability of the present active sites. The number of adsorbed arsenic ions (2.01 to 2.66) suggests the uptake of 2 or 3 ions per free site by a multi-ionic and physical mechanism considering the adsorption energy (−16.3 to −16.9 kJ/mol). The thermodynamic functions of entropy, internal energy, and free enthalpy reflect the spontaneous and exothermic properties of the studied As (V) adsorption system by CH/Al-MCM. Moreover, the composite displays significant As (V) adsorption capacity in the existence of other dissolved ions.

1. Introduction

The levels of the toxic heavy metal ions in the primary freshwater resources and water supplies have been increased to unacceptable values considering the environmental and health restrictions [1]. This occurred as a result of the significant increase in mining, industrial, and metallurgical activities [2, 3]. Most of the detected metal ions in the water supply especially at the over concentrations were categorized as toxic and carcinogenic ions that have high accumulation properties within the human and animal bodies which classify them as hazardous pollutants for humans, animals, and aquatic life [4, 5]. The arsenic ions either the trivalent arsenic (As (III)) or pentavalent arsenic (As (V)) species

were categorized as common types of heavy metal pollutants in the water resources that are of several environmental and health side effects [6, 7]. The existence of As (V) species at concentrations higher than 10 μg/L has significant carcinogenic effects on the kidney, lung, skin, and urine bladder [8, 9]. In addition, other diseases were reported for the As (V) concentrations such as vomiting, esophageal cancer, bloody diarrhea, cardiovascular disease, gastrointestinal pain, and diabetes [2, 10]. Several recommended methods were applied to diminish the detected concentrations of As (V) in water to the acceptable or recommended standards. These methods involved the membrane filtration, biological remediation, ion exchange purification, chemical precipitation, and adsorption [11, 12]. Adsorption decontamination of As (V) has been advocated in several performed studies as a simple, low-cost, and recyclable technique [1]. The recently studied adsorbents of As (V) ions included ZnO/zeolite [13], Co-Zn-ZIF [14], MWCNTs [15], Fe/biochar [9], iron oxyhydroxide [11], goethite [16], and activated carbon [7]. The preparation cost, availability of precursors, adsorption capacity, and adsorption kinetic are essential parameters to select the best adsorbent structures [8, 17, 18].

The nanoporous structures of silica that are of MCM species (MCM-41 or MCM-48) were assessed strongly as potential adsorbents for several species of metal ions and other dissolved chemicals in the water resources [19, 20]. Structurally, they are of high surficial reactivity and significant surface area as a result of their nanoporous properties and the structural active silanol groups [21]. Unfortunately, the common forms of such structures were produced based on very expensive chemicals as precursors which also exhibit toxic properties which reduce the commercial and industrial value of their different forms [21]. Therefore, introducing new or alternative precursors based on the naturally present silicate and silicate-bearing minerals and rocks was suggested to overcome the expensive cost of the traditional chemical compounds during the production of MCM silica [22, 23]. From the common natural silicate mineral, the different varieties of feldspar minerals with their alkaline aluminum silicate composition can be used as raw materials during the production of MCM nanoporous silica. They are of very wide distribution in both metamorphic and igneous rocks representing the most abundant mineral after quartz in nature [24]. K-feldspar minerals as microcline are of potassium aluminum silicate chemical structure ($KAlSi_3O_8$) which qualifies them strongly to be very suitable precursors for the fabrication of aluminum-rich mesoporous silica [23, 25].

Moreover, the controlled functionalization of the silica MCM structures with promising biopolymer chains is of significant positive impact on the textural and technical properties of MCM silica in the resulted hybrid structures [26, 27]. The prepared biopolymer/MCM composites are of multifunctional active groups, enhanced adsorption capacity, enhanced reactivity, enhanced biodegradability, and high safety [19, 28]. Chitosan as a common, biodegradable, low-cost, natural, and cationic biopolymer was recommended to form an innovative hybrid structure with MCM silica [22, 29]. Chemically, it is of polyaminosaccharide structure and exhibits several attractive technical properties such as high biodegradability, high stability, nontoxicity, high biocompatibility, and high adsorption capacity [29, 30]. Therefore, the chitosan-based structures and composites were applied extensively in the water remediation processes including both organic and inorganic dissolved chemicals as well as other medical applications such as protein delivery, gene delivery, tissue engineering, cosmetics, and drugs [29, 31].

In our previous studies, we investigate the properties of chitosan/Al-MCM-41 structure as a potential drug delivery system with enhanced loading and release properties [22]. Based on the obtained results, the structure was recommended significantly to be applied as effective adsorbents during the remediation of heavy metals and/or other toxic chemicals. Consequently, here the study introduces detailed studies about the adsorption properties of Al-MCM-41 mesoporous silica that was synthesized from natural microcline mineral and its chitosan functionalized product (chitosan/Al-MCM-41 composite) during the retention of the toxic As (V) ions from water. The effect of the chitosan chains was addressed based on the main experimental parameters, classic equilibrium studies, and the physical significance of advanced equilibrium models of statistical physics theory considering the number of active sites, occupied ion per each adsorption site, adsorption energy, and the thermodynamic functions.

2. Experimental Work

2.1. Materials. Natural microcline samples were collected from Wadi Zareib, Quseir area, Eastern Desert, Egypt, as the main precursor in the synthesis of Al-MCM-41 (Figure S1). Chemically, the microcline sample composed of SiO_2 (75.15%), Al_2O_3 (10.93%), Fe_2O_3 (2.47%), K_2O (3.468%), Na_2O (2.896%), CaO (1.975%), MgO (0.769%), TiO_2 (0.308%), P_2O_5 (0.307%), and MnO (0.307%). Cetyltrimethylammonium bromide (CTAB; 99%), chitosan (CH) powder (MW 120,000; 85%), sodium hydroxide (97%), ethanol (95%), and hydrochloric acid (HCl) were delivered from Sigma-Aldrich, Egypt, as the required chemical during the synthesis processes. Arsenic (As (V)) standard solution of 1000 mg/L concentration was used as stock during the preparation of the polluted solutions at different concentrations.

2.2. Synthesis of Al-MCM-41. The synthesis procedures were conducted based on the reported method by Chen et al. [23]. After grinding the microcline sample to a size range from 15 μm to 100 μm, the obtained fractions were heated for 8 h at 850°C as a step to destruct its crystalline framework. After that, the heated sample (5 g) was treated with HCl solution (150 mL) of 5 M concentration at 85°C for 4 h. After washing the treated sample from the remaining HCl solution, 0.3 g of the leached fractions were

mixed with the solid pellets of NaOH (1 : 1 ratio), and the mixture was heated at 100°C for 2 h. The fused microcline/NaOH mixture was ground, mixed with distilled water (50 mL), and stirred for 12 h under room temperature. Then, the product was mixed with 10 mL of CTAB solution (0.5 g) at adjusted conditions of pH 9 and 65°C for 2 h. The new mixture was hydrothermally treated in Teflon lined stainless-steel autoclave at 110°C for 24 h. After cooling, the synthetic Al bearing MCM-41 fractions were extracted from the residual solutions, washed with ethanol as well as distilled water, and dried at 80°C for about 12 h. Finally, the synthetic Al-MCM particles were heated for 6 h at 550°C to remove used CTAB molecules and the product was labeled as Al-MCM.

2.3. Synthesis Chitosan/Al-MCM-41 Nanocomposite (CH/Al-MCM). The integration between the prepared Al-MCM and chitosan was performed by a simple method based on the reported procedures by Jiang et al. [19]. About 3 g of the synthetic Al-MCM was homogenized with a certain volume of distilled water (50 mL) for 180 min in the existence of a sonication source (240 W). At the same time, the chitosan solution was prepared by dissolving 3 g of the polymer powder in acetic acid of 0.1 M (50 mL). After that, the chitosan solution was mixed with the Al-MCM suspension and the resulted mixture was stirred for 12 h under the effect of the sonication irradiation (240 W). After this period, the resulted particles of CH/Al-MCM were extracted by a filtration process, washed carefully to avoid the effect of the rest acetic acid, and finally dried for 12 h at 60°C.

2.4. Characterization Techniques. The crystal phases and crystal structures were studied based on the low angle XRD patterns (1° to 10°) and high angle patterns (5° to 70°) by X-ray diffractometer (PANalytical (Empyrean)) to confirm the successful conversion of microcline into the mesoporous structure and structural impacts of the integrated chitosan. The chemical structures were studied based on the FT-IR spectra of the materials within the determination frequency range from 400 cm^{-1} to 4000 cm^{-1} by Fourier-transform infrared spectrometer (Shimadzu; FTIR-8400S). This analysis supports the structural findings according to the XRD analysis as it reflects the possible chemical interaction between the integrated components which cannot be determined strongly based on the XRD patterns. The surficial features and the material forms were studied by scanning electron microscope (Gemini, Zeiss-Ultra 55). The internal structures and features were addressed by a high-resolution transmission electron microscope (JEOL-JEM2100). The morphological studies also confirm the formation of the composite and support the XRD and FT-IR findings in addition to their significance on the textual and microstructural properties. The microstructural studies such as the surface area and porosity of Al-MCM and CH/Al-MCM were measured using a surface area analyzer (a Beckman Coulter SA3100) as essential and effective parameters during the application of Al-MCM and CH/Al-MCM as adsorbents.

2.5. Adsorption Studies. The performed tests were designed according to experimental variables of the batch studies considering the experimental influence of pH (2–7), dosages (0.1–0.5 g/L), uptake contact time (30–1020 min), temperature (20–40°C), As (V) concentration (50–400 mg/L), and certain volume (200 mL). Each experiment was repeated three times, and the determined results were presented in their averages achieving standard deviations less than 4.7%. The treated solutions by both Al-MCM and CH/Al-MCM were acidified using diluted nitric acid (2%), and the rest concentrations of As (V) were measured by inductively coupled plasma mass spectrometry (Perkin Elmer). The As (V) adsorption capacity (Q_e) was estimated based on the following equation:

$$Q_{e\,(mg/g)} = \frac{(C_o - C_e)V}{m}, \tag{1}$$

where Q_e is the estimated As (V) adsorption capacity in mg/g, C_o is the starting As (V) concentration in mg/L, C_e is the rest As (V) concentration in mg/L, m is the adsorbent dosage in g, and V is the volume of the As (V) solution in mL. The determination coefficient (R^2) and chi-squared test (χ^2) were assessed during the evaluation of the classic isotherm and kinetic nonlinear equations (Table S1) considering equations (2) and (3), respectively.

$$R^2 = 1 - \frac{\sum\left(q_{e,\,\mathrm{exp}} - q_{e,\mathrm{cal}}\right)^2}{\sum\left(q_{e,\,\mathrm{exp}} - q_{e,\mathrm{mean}}\right)^2}, \tag{2}$$

$$\chi^2 = \sum \frac{\left(q_{e,\,\mathrm{exp}} - q_{e,\mathrm{cal}}\right)^2}{q_{e,\mathrm{cal}}}. \tag{3}$$

For the studied advanced equilibrium models based on the statistical physics theory assumptions (Table S1), the root mean square error (RMSE) was used to detect the fitting degree according to equation (4) in addition to the values of correlation coefficient (R^2) values.

$$\mathrm{RMSE} = \sqrt{\frac{\sum_{i=1}^{m}\left(Qi_{\mathrm{cal}} - Qi_{\mathrm{exp}}\right)^2}{m' - p}}, \tag{4}$$

where m, Qi_{cal}, Qi_{exp}, and p symbols in the equation denate the experimental data, As (V) adsorbed quantity, actual As (V) adsorbed quantity, and number of the assessed variables, respectively.

3. Results and Discussion

3.1. Characterization of the Adsorbents. Based on the XRD results, the low angle patterns of both Al-MCM-41 and CH/Al-MCM declare the existence of three dominant peaks 2.4° (100), 3.65° (110), and 4.52° (200) which signifies the high order mesoporous structure of MCM-41 (JCPDS 00-049-1712) (Figures 1(a) and 1(b)). The deviation in these peaks in the pattern of CH/Al-MCM suggested the effect of the integrated chitosan chains and their interaction with the silanol active groups of the Al-MCM substrate (Figure 1(b)).

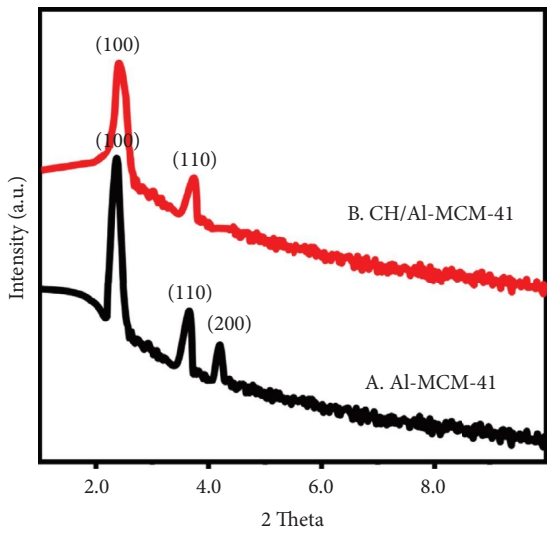

Figure 1: Low angle XRD patterns of synthetic Al-MCM (A) and CH/Al-MCM composite (B).

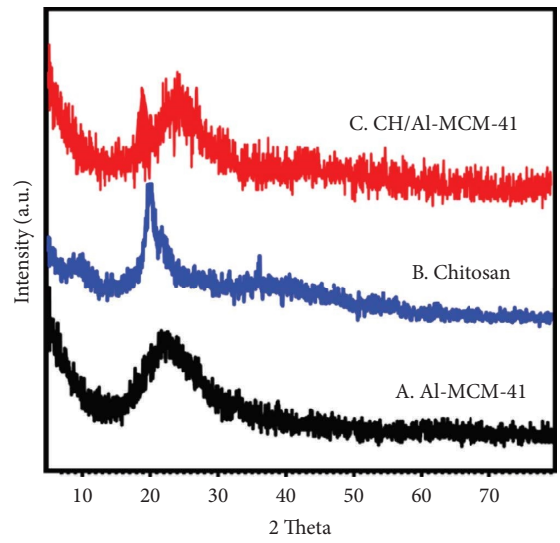

Figure 2: High angle XRD patterns of synthetic Al-MCM (A), integrated chitosan (B), and CH/Al-MCM composite (C).

The high angle pattern of the synthetic Al-MCM-based materials as compared to microcline precursor demonstrates the successful transformation of the crystalline structure of microcline into the semicrystalline structure of MCM-41 (Figure 2). The pattern of Al- MCM, as well as CH/Al-MCM, appeared as the common patterns of amorphous silica with a broad peak around 22.5° (Figure 2). The pattern of CH/Al-MCM shows deviated and much reduced peak at about 20.2° which identifies the integrated chitosan considering the pattern of the raw chitosan powder (Figure 2).

The morphological studies declared the formation of Al-MCM-based microcline in elliptical or spherical forms which was reported commonly to the mesoporous silica of MCM-41 type (Figure 3(a)). For the prepared CH/Al-MCM composite, the Al-MCM particles were recognized to be coated with fibers or lenticular grains which is related to the chitosan component of the composite (Figures 3(b) and 3(c)). The TEM images for the spherical grains for Al-MCM declared the hexagonal pores of MCM-41 (Figure 3(d)). The HRTEM images of the CH/Al-MCM composite reflect the existence of the Al-MCM as inclusion within the lenticular particle of chitosan (Figures 3(e) and 3(f)). The high magnification of CH/Al-MCM demonstrates the porous properties of the enclosed Al-MCM grains (Figures 3(e) and 3(f)). The morphological properties have a strong impact on the textural and microstructural properties. There is a considerable increase in the surface area (935 m^2/g for Al-MCM and 942 m^2/g for CH/Al-MCM) and the pore diameter (2.73 nm for Al-MCM and 3.42 nm for CH/Al-MCM). This signifies the effect of the integrated chitosan as the fibrous habit of its particles, and the porosity of its polymeric matrix causes enhancement of the surface area and increases in the average pore diameter.

The FT-IR spectrum of CH/Al-MCM was compared with the spectra of chitosan and Al-MCM (Figure 4). The spectrum of Al-MCM displays the identification band of mesoporous silica (Si-O-) at 457.1 cm^{-1} in addition to other common bands at 810 cm^{-1} (symmetric Si-O-Si), 963 cm^{-1} (Si-O-Al), 1075 cm^{-1} (asymmetric Si-O-Si), and 3735 cm^{-1} (silanol groups) [20, 32, 33] (Figure 4(a)). The spectrum of CH/Al-MCM (Figure 4(c)) exhibits the same bands but at shifted positions in addition to other new bands that are related to the reported chemical structure of the functionalized chitosan (Figure 4(b)). The recognized chemical groups that signify the chitosan structure in the spectrum of CH/Al-MCM are C-O (1084 cm^{-1}), C-H (1375 cm^{-1}), and N-H (1492 cm^{-1}) [30] (Figure 4(c)). This reflects the formation of the composite based on the interaction between the active MCM-41 silanol groups and N-H as well as C=O groups of chitosan by forming a chemical complex as the absorption bands of these groups were consumed strongly after the integration reactions.

3.2. Adsorption Results

3.2.1. Effect of Adsorption pH. The influence of solution pH as experimental variable was assessed from pH 2 until pH 7 at certain values for the other parameters (concentration (100 mg/L), volume (200 mL), time (120 min), dosage (0.1 g/L), and temperature (20°C)). The determined As (V) sequestration results either by Al-MCM or by CH/Al- MCM with the increment in the pH of the solutions up to pH 6 (36.8 mg/g (Al-MCM) and 54.6 mg/g (CH/Al- MCM)) (Figure 5). Beyond this pH value (pH 6), the addressed adsorbents display observable adverse behavior, and the estimated capacities declined significantly (Figure 5). The previous adsorption behaviors as a function of the solution pH were illustrated considering the speciation properties of As (V) ions as well as the surface properties of both Al-MCM and CH/Al-MCM. The speciation diagram of As (V) demonstrates its existence in neutral form (H_3AsO_4) within pH range from pH 2 to pH 3 and acidic forms from pH 3 to pH 12 ($H_2AsO_4^-$ (pH 4 to 5.5), $HAsO_4^{2-}$, and AsO_4^{3-} (PH 7 to 12)) [34–36]. Considering such speciation behaviors of As (V) and the predicted deprotonation of the reactive

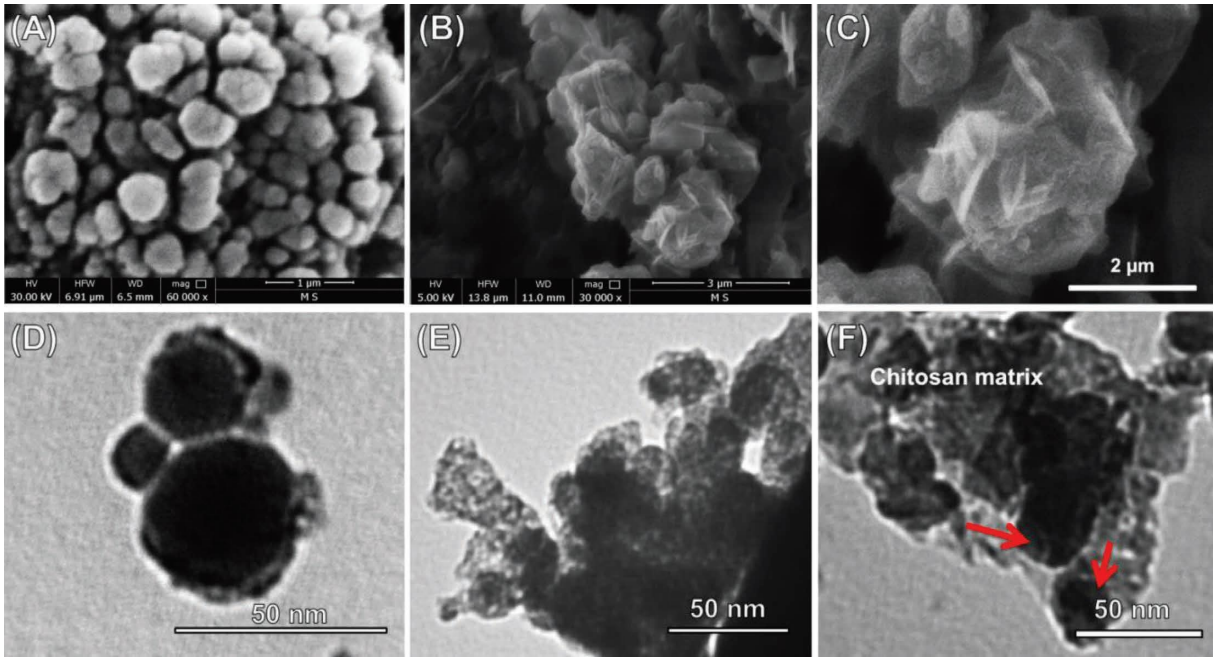

Figure 3: SEM image of the prepared Al-MCM (A), SEM image CH/Al-MCM composite (B, C), HRTEM image of Al-MCM (D), and HRTEM images of the CH/Al-MCM composite (E, F).

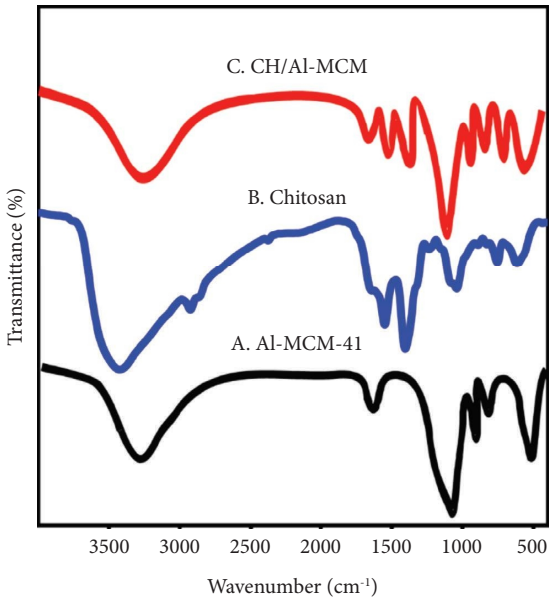

Figure 4: FT-IR spectra of the prepared Al-MCM (A), integrated chitosan (B), and CH/Al-MCM composite (C).

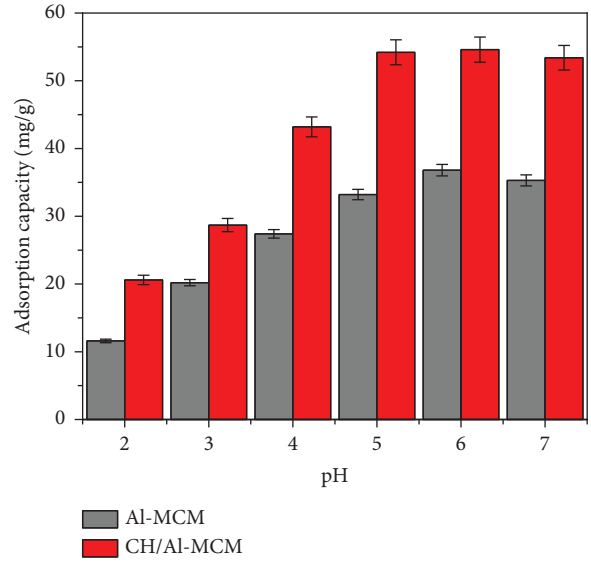

Figure 5: The determined As (V) retention capacities of Al-MCM and CH/Al-MCM at the different studied pH values.

functional groups of Al-MCM (silanol units (Si-OH)) and CH/Al- MCM (Si-OH, N-H, OH, C-N, and C=O) by increasing the pH value, pH 6 achieve the best retention properties as the structures still exhibit the satisfying positive charges that can provide effective electrostatic attractive forces with the acidic As (V) ions. At the neutral to high pH conditions, the enrichment of the Al-MCM and CH/Al-MCM structures in negatively charged hydroxyl ions causes significant repulsion of the interaction As (V) ions which also are of acidic forms [2].

3.2.2. Kinetic Studies

(1) Time Interval. The As (V) adsorption properties as a function of the addressed time intervals were studied within a tested range from 30 min to 1020 min at certain values for the other parameters (concentration (100 mg/L), volume (200 mL), pH (6), dosage (0.1 g/L), and temperature (20°C)). The As (V) uptake processes by Al-MCM and CH/Al-MCM exhibit observable segmental curves with time (Figure 6(a)). The segmental form of the curves is related to two different As (V) uptake rates; the first segment or

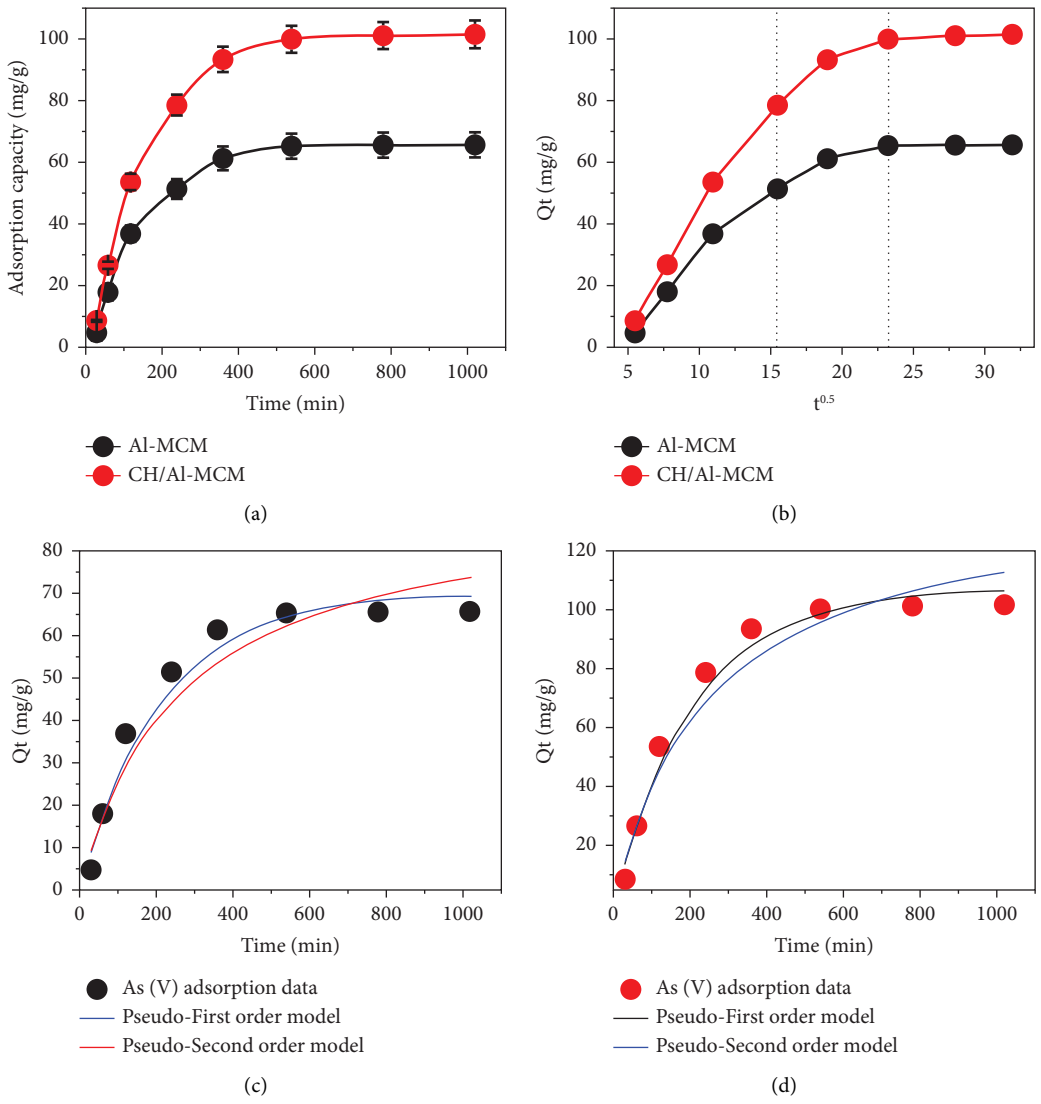

Figure 6: The change in the As (V) retention capacities of Al-MCM and CH/Al-MCM with the contact time (a), intra-particle-diffusion curves of Al-MCM and CH/Al-MCM composite (b), fitting of retention results of As (V) with the kinetic models using Al-MCM (c), and fitting of retention results of As (V) with the kinetic models using CH/Al-MCM (d).

portion is associated with a rapid As (V) uptake rate which can be detected up to 540 min either for Al-MCM or CH/Al-MCM (Figure 6(a)). This is followed by another stage which appears in the second segment characterized by a fixed or neglected As (V) uptake rate of no obvious increase in the actual uptake capacity and attends an equilibration state (65.6 mg/g (Al-MCM) and 101.4 mg/g (CH/Al-MCM)) (Figure 6(a)). The retention or adsorption equilibration states of Al-MCM and CH/Al-MCM were attended as a result of the significant and continuous occupation of their effective receptors or active sites with the adsorbed As (V) ions which reduce the actual retention rates with time until the full saturation of all the present sites with the adsorbed metal ions [2].

(2) Intra-Particle-Diffusion Behavior. The plotted intra-particle-diffusion curves of both Al-MCM and CH/Al-MCM as applied adsorbents for As (V) ions exhibit observable segmental properties without detection for the intersection between the curves and the original points. This suggested the operation of more than one As (V) adsorption mechanism in addition to the diffusion processes of its dissolved ions [2] (Figure 6(b)). The detected segments can be classified into three portions considering the slope of the curves. The initially recognized segment that covers the starting sequestration intervals is related to retentions of arsenic (As (V)) by the external or the surficial free active receptors or sites of Al-MCM and CH/Al-MCM (Figure 6(b)). The identification of the second segment reflects the significant vanishing of surficial uptake mechanisms and the operation of the layered adsorption processes [37] (Figure 6(b)). The finally detected segment appears to cover the adsorption intervals of the equilibration stage. The recognition of this segment demonstrates the operation of interionic attraction in addition to/or molecular association processes as the affecting sequestration mechanisms [37].

(3) Kinetic Modeling. The kinetic behaviors and properties of Al-MCM and CH/Al-MCM adsorption systems during the sequestration of arsenic (As (V)) from water were discussed according to the recognized nonlinear fitting degrees (correlation coefficient (R^2) and chi-squared test (χ^2)) between the uptake results and the kinetic assumptions of pseudo-first order (P.F) and pseudo-second order (P.S) models (Figures 6(c) and 6(d)). The recognized values of R^2, as well as χ^2, validate significant agreement for the uptake of As (V) by Al-MCM and CH/Al-MCM with the kinetic assumption of the P.F model as compared to the kinetic behavior of the P.S model (Figures 6(c) and 6(d); Table 1). The kinetic assumption and properties of the P.F model suggest the retention of the dissolved ions by types of physisorption mechanisms [17, 38]. However, the observed significant fitting with the kinetic equations of the P.S model suggests a considerable impact on some chemisorption processes such as chemical bonding, chemical complexes, and electron sharing [1].

3.2.3. Equilibrium Studies

(1) As (V) Concentration. The adsorption behaviors of Al-MCM and CH/Al-MCM using different starting As (V) concentrations were assessed within an experimental range from 50 mg/L to 400 mg/L considering the change in the temperature conditions from 20°C until 40°C. This was completed at certain values for the other parameters (time (24 h), volume (200 mL), pH (6), dosage (0.1 g/L), and temperature (20°C)). The experimentally measured As (V) retention capacities by Al-MCM and CH/Al-MCM were enhanced at a remarkable rate at the high starting concentrations of the arsenic ions (Figure 7(a)). This enhanced effect is credited to the expected acceleration in the diffusion and driving forces of As (V) under the saturation of the solutions with its dissolved ions which induce the interaction chances between the surfaces of Al-MCM and CH/Al-MCM and the arsenic ions [2]. The increment in the Al-MCM and CH/Al-MCM uptake capacities as adsorbents of As (V) ions was detected as a function of the tested concentrations until certain concentrations which are the equilibrium concentrations (Figure 7(a)). The equilibrium concentrations for the uptake of As (V) by Al-MCM are 300 mg/L (20°C and 30°C) and 350 mg/L (40°C) (Figure 7(a)). For CH/Al-MCM, the recognized equilibrium concentrations are 250 mg/L at the addressed three retention temperature values. The determined adsorption campsites of As (V) at these concentrations are the maximum capacities that can be achieved experimentally. The determined As (V) maximum retention capacities by Al-MCM at 20°C, 30°C, and 40°C are 115 mg/g, 84 mg/g, and 71.2 mg/g, respectively (Figure 7(a)). For CH/Al-MCM, the estimated maximum capacities are 170.4 mg/g, 110.6 mg/g, and 80.8 mg/g at a studied temperature of 20°C, 30°C, and 40°C, respectively (Figure 7(a)). The previously reported findings declare a significant positive effect for the functionalized chitosan on the As (V) adsorption properties of Al-MCM either by prompting the surface area and/or providing additional adsorption active functional groups.

(2) Classic Isotherm Modeling. The equilibrium behaviors of the Al-MCM and CH/Al-MCM adsorption systems of As (V) were described considering the nonlinear fitting processes of the obtained results with the equilibrium and isotherm assumptions of the commonly studied Langmuir (L.G) (Figures 7(b) and 7(d)), Freundlich (F.E) (Figures 7(c) and 7(e)), and Dubinin–Radushkevich (D-R) models (Figures 7(f) and 7(g)) as well as their theoretical parameters. According to the recognized R^2 and χ^2 values, the adsorption of arsenic by both Al-MCM and CH/Al-MCM follows the equilibrium assumption and properties of Langmuir isotherm rather than the reported properties of Freundlich isotherm (Table 1). This validates the retention of the arsenic metal (As (V) in homogenous and monolayer forms [39]. The estimated theoretical As (V) Q_{max} values considering the best reaction temperature (20°C) are 125.4 mg/g and 202.6 mg/g for Al-MCM and CH/Al-MCM, respectively, (Table 1). Based on the estimated Gaussian energy as theoretical parameters for the fitting processes of the As (V) adsorption results with the D-R model, the uptake reactions either by Al-MCM (4.6–5.3 kJ/mol) or CH/Al-MCM (2.8–4.4 kJ/mol) are within the reported range for the physisorption processes (<8 kJ/mol) (Table 1) [2].

(3) Advanced Isotherm Models. A monolayer model with one energy site was assessed to illustrate the equilibrium properties of the performed As (V) uptake processes either by Al-MCM (Figure 7(h)) or CH/Al-MCM (Figure 7(i)) according to the advanced assumption of the statistical physics theory (Table 1). The main mathematical fitting parameters which were estimated are the steric parameters (n (number of adsorbed arsenic ions per each site), Nm (the active site's density of Al-MCM and CH/Al-MCM), and Q_{sat} (the As (V) uptake capacity during the saturation state of the used adsorbents)) and energetic parameters (ΔE (the adsorption energy of As (V)), G (enthalpy), Sa (entropy), and E_{int} (internal energy)) (Table 1).

(i) Steric parameters

(a) Number of adsorbed arsenic ions per site (n): The number of adsorbed arsenic ions per active site (n parameter) is of promising significance to the uptake mechanism in addition to the predicted orientation and/or forms of the adsorbed arsenic by Al- MCM and CH/Al-MCM. Generally, the obtained values of n are higher than 1 either for Al-MCM ($n = 2.02$–2.31) or CH/Al-MCM ($n = 2.02$–2.66) which suggests the orientation of the adsorbed arsenic ions in vertical or non-parallel orientation (Figure S1; Table 1). Moreover, there are two or three arsenic ions that can be adsorbed per effective receptor or site by types of multi-ionic mechanisms [40, 41]. Regarding the temperature impact on the values of n parameters of Al-MCM, the values increased linearly with the elevation in the tested temperature from 293 K ($n = 2.02$) to 313 K ($n = 2.31$) reflecting a significant increase in the aggregation affinities of the adsorbed arsenic ion (Figure8(a);

Table 1: The theoretically obtained mathematical parameters of the evaluated kinetic models, classic isotherm models, and advanced isotherm models.

Materials	Models	Parameters	Values		
Kinetic models					
Al-MCM	Pseudo-first-order	K_1 (1/min)	0.0046		
		$Q_{e(\mathrm{Cal})}$ (mg/g)	69.8		
		R^2	0.96		
		X^2	1.122		
	Pseudo-second-order	K_2 (1/min)	4.1×10^{-5}		
		$Q_{e(\mathrm{Cal})}$ (mg/g)	92.4		
		R^2	0.94		
		X^2	1.69		
CH/Al-MCM	Pseudo-first-order	K_1 (1/min)	0.0047		
		$Q_{e(\mathrm{Cal})}$ (mg/g)	106		
		R^2	0.97		
		X^2	1.003		
	Pseudo-second-order	K_1 (mg/min)	2.83×10^{-5}		
		$Q_{e(\mathrm{Cal})}$ (mg/g)	140.3		
		R^2	0.95		
		X^2	1.74		
			293 K	303 K	313 K
Parameters of the classic isotherm models					
Al-MCM	Langmuir model	$Q_{\max}$ (mg/g)	125.4	90.7	82.8
		B (L/mg)	0.0054	0.00188	0.0011
		R^2	0.95	0.93	0.93
		X^2	0.98	1.65	1.43
	Freundlich model	$1/n$	0.56	0.80	0.89
		k_F (mg/g)	4.64	0.83	0.41
		R^2	0.88	0.90	0.91
		X^2	2.22	2.4	2.02
	D-R model	β (mol^2/kJ^2)	0.0236	0.021	0.0177
		Q_m (mg/g)	113	83.5	72
		R^2	0.97	0.96	0.96
		X^2	0.57	0.84	0.85
		E (kJ/mol)	4.6	4.87	5.3
CH/Al-MCM	Langmuir model	$Q_{\max}$ (mg/g)	202.6	183.2	102.5
		B (L/mg)	0.0069	0.004	0.0035
		R^2	0.95	0.90	0.91
		X^2	1.47	2.7	1.82
	Freundlich model	$1/n$	0.5	0.64	0.66
		k_F (mg/g)	7.41	2.87	1.77
		R^2	0.86	0.84	0.85
		X^2	3.4	4.37	2.92
	D-R model	β (mol^2/kJ^2)	0.063	0.048	0.025
		Q_m (mg/g)	169.2	113.5	82
		R^2	0.97	0.99	0.99
		X^2	0.68	0.15	0.19
		E (kJ/mol)	2.8	3.2	4.4
Steric and energetic parameters of the advanced isotherm model					
Al-MCM		R^2	0.998	0.996	0.997
		N	2.02	2.25	2.31
		Nm (mg/g)	61.53	40.43	33.54
		Q_{Sat} (mg/g)	124	91.2	77.8
		C1/2 (mg/L)	84.88	116.03	129.03
		ΔE (kJ/mol)	−16.03	−15.78	−16.03
CH/Al-MCM		R^2	0.996	0.994	0.997
		N	2.01	2.66	2.54
		Nm (mg/g)	88.86	46.69	38.3
		Q_{Sat} (mg/g)	178.6	124.2	98.5
		C1/2 (mg/L)	74.15	83.7	89.58
		ΔE (kJ/mol)	−16.36	−16.6	−16.98

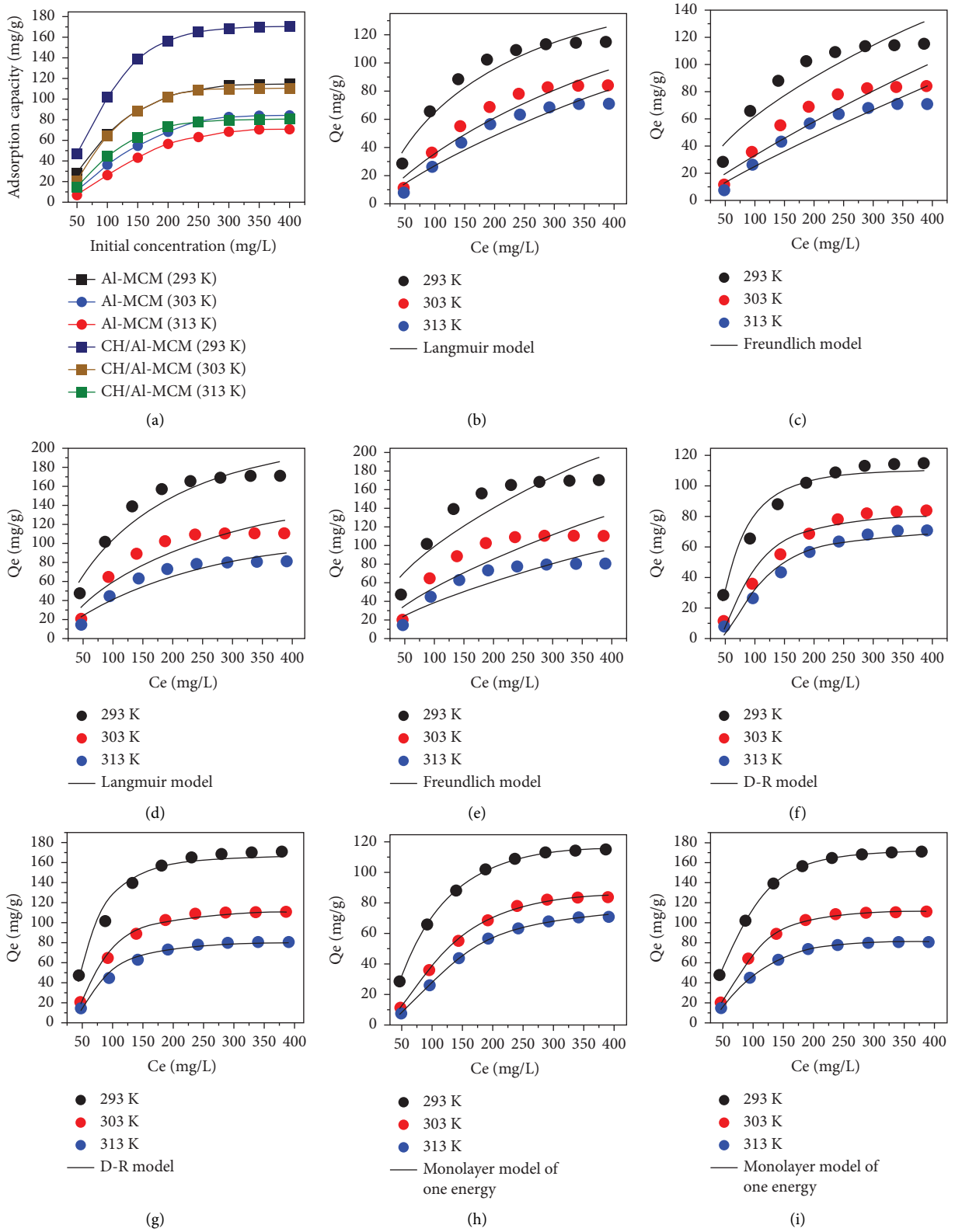

Figure 7: The adsorption behaviors of Al-MCM and CH/MCM at different started concentrations of As (V) and at different temperature (a), fitting of the As (V) uptake results by Al-MCM with Langmuir model (b), fitting of the As (V) uptake results by Al-MCM with Freundlich model (c), fitting of the As (V) uptake results by CH/Al-MCM with Langmuir model (d), fitting of the As (V) uptake results by CH/Al-MCM with Freundlich model (e), fitting of the As (V) uptake results by Al-MCM with D-R model (f), fitting of the As (V) uptake results by CH/Al-MCM with D-R model (g), fitting of the As (V) uptake results by Al-MCM with monolayer model of one energy (h), and fitting of the As (V) uptake results by CH/Al-MCM with monolayer model of one energy (i).

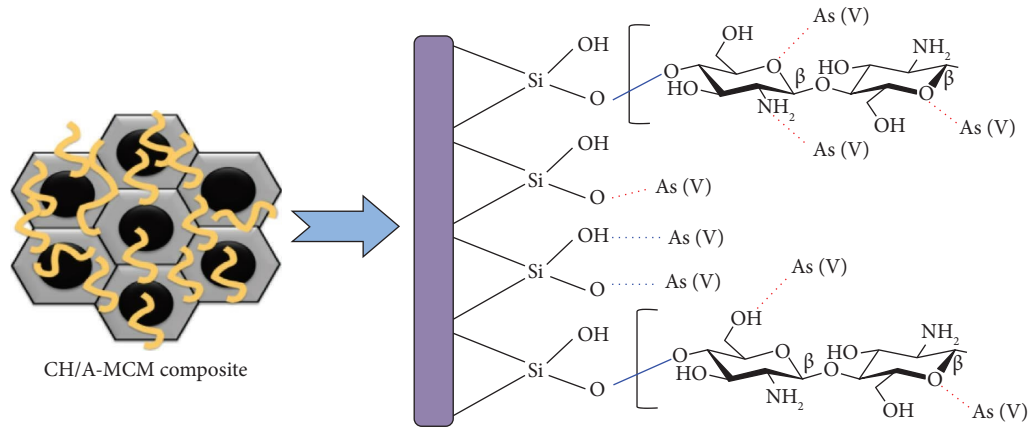

Figure 8: Schematic diagram for the adsorption mechanism of As (V) by CH/Al-MCM composite.

Table 1). The predicted augmentation in the arsenic aggregation validates the impact of the thermal or energetic activation on the adsorption system prior to the chemical interactions between AS (V) and the reactive receptors of Al-MCM. For CH/Al-MCM, the values of the n parameter increased significantly with the temperature from 293 K ($n = 2.01$) to 303 K ($n = 2.66$) and then declined again after adjusting the temperature at the higher value (313 K; $n = 2.54$) (Figure 8(a); Table 1). This behavior might be related to the expected changes in quantities and types of the effective receptors of the arsenic ions with the experimental change in the temperature conditions [41, 42].

(b) Density of the occupied active sites (Nm): The Nm steric mathematical parameter denotes the occupied active site densities of Al-MCM and CH/Al-MCM during the sequestration of dissolved arsenic (As (V)). The recognized Nm values of CH/Al-MCM at all the inspected temperature (Nm = 88.8 mg/g (293 K), 46.9 mg/g (303 K), and 38.8 mg/g (313 K)) are higher than Al-MCM (Nm = 61.5 mg/g (293 K), 40.4 mg/g (303 K), and 33.5 mg/g (313 K)) (Figure 8(b); Table 1). This reveals the enhancement impact of the functionalization process with chitosan chains on the quantities of free and effective receptors by providing the formed structure of new types of active functional groups. Regarding the actual impact of the adsorption temperature, the recognized Nm values either for Al-MCM or CH/Al-MCM declined strongly with the elevation in the tested temperature from 293 K until 313 K (Figure 8(b); Table 1). This behavior is a predicted result of the remarkable increase in the arsenic aggregation properties and the predicted deactivation effect of high-temperature conditions (313 K) on the chitosan active site [41].

(c) Adsorption of arsenic at the saturation state (Q_{sat}): The As (V) Q_{sat} values of Al-MCM and CH/Al-MCM are controlled by the reported numbers of the adsorbed arsenic and/or the active sites' densities. Generally, the Q_{sat} values of both Al-MCM and CH/Al- MCM declined strongly by increasing the experimental temperature values from 293 K to 313 K (Figure 8(c); Table 1). The determined values by Al-MCM are 124.3 mg/g, 91.2 mg/g, and 77.8 mg/g at the studied temperature of 293 K, 303 K, and 313 K, respectively, (Figure 8(c); Table 1). The obtained values using the CH/Al- MCM composite are 178.6 mg/g, 124.2 mg/g, and 98.5 mg/g at temperatures of 293 K, 303 K, and 313 K, respectively, (Figure 8(c); Table 1). The recognized variations in the calculated values of Q_{sat} values with the studied experimental temperature exhibit the same trends of the Nm values. Therefore, the arsenic adsorption capacities of Al-MCM and CH/Al-MCM depend mainly on the quantities of the distributed effective receptors. This illustrates the reported higher As (V) uptake capacity of CH/Al-MCM than Al-MCM as single components.

(i) Energetic Properties

(a) Adsorption energy (ΔE): The adsorption energies (ΔE) of Al-MCM and CH/Al-MCM adsorption systems for As (V) reflect the controlling mechanism. The adsorption energies were calculated based on equation (5) where the presented symbols of ΔE, R, T, S, and C denate the As (V) adsorption energy, gas constant, absolute temperature, the solubility of As (V) salt, and the concentration of the arsenic ions at the half-saturation state [41].

$$\Delta E = RTln\left(\frac{S}{C}\right). \quad (5)$$

The adsorption systems that display ΔE less than 40 kJ/mol elaborate the operation of physical mechanisms including hydrogen bonding (<30 kJ/mol), van der Waals forces (4–10 kJ/mol), hydrophobic bonding (5 kJ/mol), coordination exchange process (40 kJ/mol), and dipole bonding forces (2–29 kJ/mol) [41, 43]. The obtained ΔE values of Al-MCM (15.8 to 16.03 kJ/mol) and CH/Al-MCM (16.3 to 17 kJ/mol) are within the reported range for the physical adsorption processes (Table 1). Also, the values suggested complex hydrogen bonding (<30 kJ/mol) and dipole bonding forces (2–29 kJ/mol) as the effective mechanism. The negative signs of the estimated ΔE values of Al-MCM or CH/Al-MCM during the arsenic adsorption validate the exothermic properties of the two systems [44]. The suggested retention mechanism of As (V) by CH/Al- MCM was presented graphically in Figure 9 considering the main effective chemical groups.

(ii) Thermodynamic Functions

1 Entropy (Sa): The entropy (Sa) of the arsenic uptake reactions using Al-MCM and CH/Al-MCM as adsorbents considering the assessed As (V) concentration as well as the experimental temperature validates significantly the order and/or disorder properties of the inspected adsorbents. The obtained values of entropy were estimated directly from equation (6) [44].

$$\frac{S_a}{K_B} = Nm\left\{\ln\left(1+\left(\frac{C}{C_{(1/2)}}\right)^n\right) - n\left(\frac{C}{C_{(1/2)}}\right)^n \frac{\ln\left(C/C_{(1/2)}\right)}{1+\left(C/C_{(1/2)}\right)^n}\right\}. \quad (6)$$

The estimated trends of Sa values at the addressed As (V) concentrations decrease at a remarkable rate with testing the high arsenic concentrations (Figures 8(d) and 8(e)). This reflects recognizable intensification in the surficial disorder properties of Al-MCM and CH/Al-MCM during the interactions between their surfaces and the arsenic ions. Moreover, this suggests significant docking of the adsorbed arsenic on the effective and free receptors of Al-MCM and CH/Al-MCM at the tested low concentrations of As (V) [41, 42]. For Al-MCM, the entropy exhibits its maxima values at equilibrium concentrations of 91.8 mg/L (293 K), 143 mg/L (303 K), and 144.58 mg/L (313 K) (Figure 8(d)). For CH/Al-MCM the maxima entropy values were recognized at the equilibrium concentrations of 87.3 mg/L (293 K), 91.95 mg/L (303 K), and 94.4 mg/L (313 K) (Figure 8(e)). The previous values are close to recognized concentrations of arsenic at the half-saturation (C1/2) states of Al- MCM as well as CH/Al-MCM. This proves the full saturation of these effective receptors with the adsorbed As (V) at these equilibrium concentrations and in turn no more ions might be docked into these sites. Beyond the previous concentrations, the Sa values declined strongly reflecting the remarkable drop in the effective receptors and diffusion behavior of As (V) ions as well as their freedom degrees [40].

(2) Internal Energy (E_{int}) and Free Enthalpy (G): The internal energies of Al-MCM and CH/Al-MCM adsorption systems for As (V) were determined based on equation (7) considering the translation partition value per unit volume (Z_v) [44].

$$\frac{E_{\text{int}}}{K_B T} = nN_m\left[\left(\frac{\left(C/C_{(1/2)}\right)^n \ln\left(C/Z_v\right)}{1+\left(C/C_{(1/2)}\right)^n}\right) - \left(\frac{n\ln\left(C/C_{1/2}\right)\left(C/C_{1/2}\right)^n}{1+\left(C/C_{(1/2)}\right)^n}\right)\right]. \quad (7)$$

The obtained internal energies (E_{int}) of Al-MCM and CH/Al-MCM display negatively signed values which are associated with the reactions that exhibit spontaneous properties at all the assessed As (V) concentrations and experimentally adjusted temperature (Figures 8(f) and 8(g)). The distinguished diminution in the E_{int} values with the uptake temperature from 293 K to 313 K proves the adsorption of As (V) by exothermic reactions either by Al-MCM (Figure 8(f)) or CH/Al-MCM (Figure 8(g)). In addition, determining the free enthalpy (G) based on equation (8) as negative values at the assessed arsenic concentrations and experimental temperature values confirm the previously recognized findings according to the E_{int} values (Figures 8(h) and 8(i)). The uptake of dissolved arsenic ions by both Al-MCM and CH/Al-MCM occurred by spontaneous reactions. Moreover, the recognized decline in the calculated G values with the experimental temperature reflects a significant fall in the feasibility properties of the arsenic uptake reactions at high-temperature conditions (Figures 8(h) and 8(i))

$$\frac{\text{G}}{K_B T} = nN_m \frac{\ln\left(C/Z_v\right)}{1+\left(C_{1/2}/C\right)^n}. \quad (8)$$

3.2.4. Effects of Coexisting Ions. The As (V) adsorption efficiency by CH/Al-MCM was studied considering the effects of the other dissolved metals (Cd (II), Pb (II), Ni (II), and Co (II)) and chemical anions (NO^-, PO^{3-}, SO^{2-}, and CO^{2-}). The experimental variables were adjusted at 24 h as equilibrium time, 400 mg/L as tested concentration, 200 mL as the studied volume, 0.1 g/L as the used CH/Al-MCM dosage, 20°C as the temperature of the test, and pH 6. The determined results demonstrate neglected or slight adverse

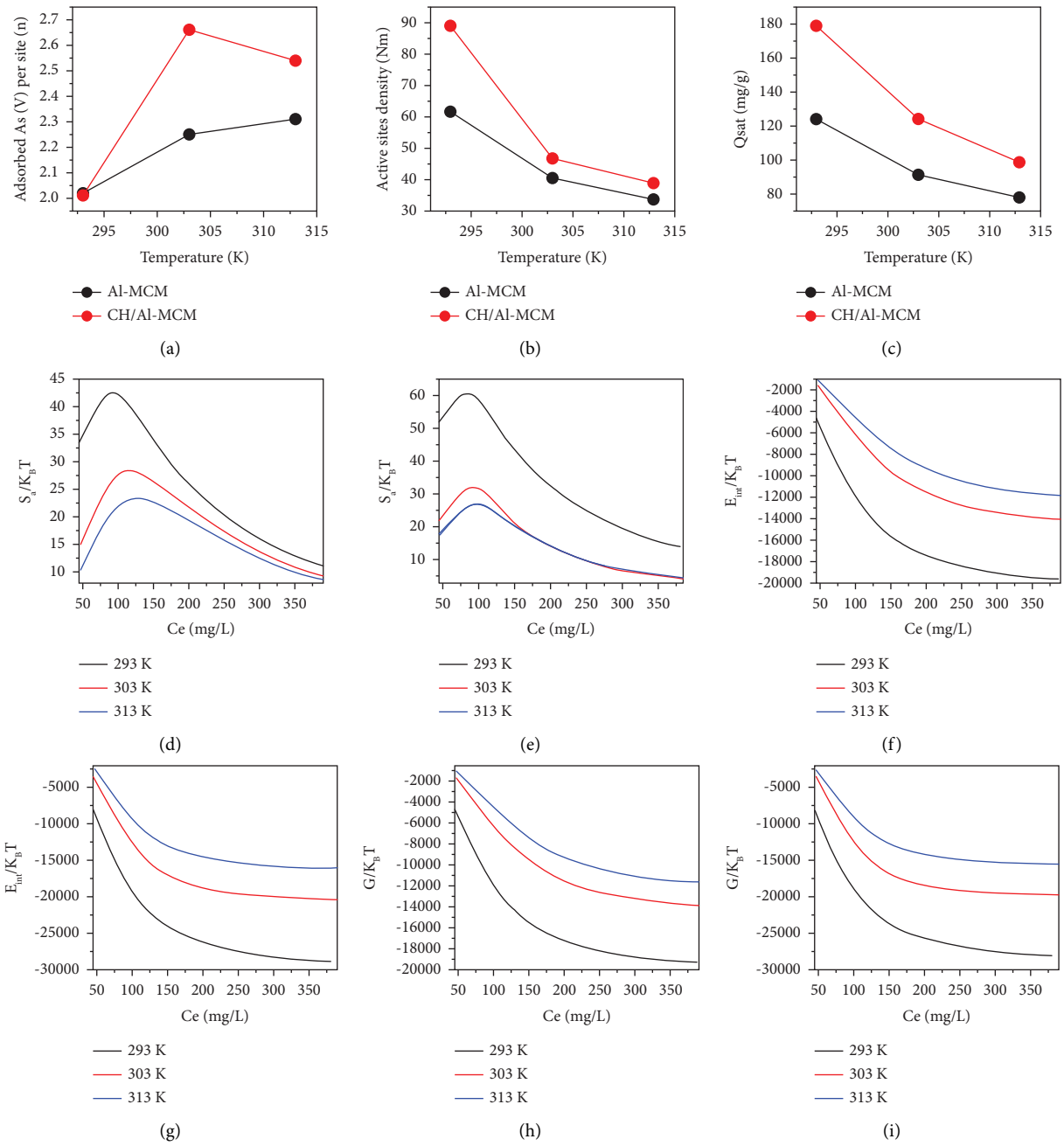

Figure 9: The theoretical variation in the adsorbed As (V) per site (a), change in adsorption sites density (b), change in the As (V) Qsat values (c), change in the entropy of Al-MCM adsorption system (d), change in the entropy of CH/Al-MCM adsorption system (e), change in the internal energy of Al-MCM adsorption system (f), change in the internal energy of CH/Al-MCM adsorption system (g), change in the enthalpy of Al-MCM adsorption system (h), and change in the enthalpy of CH/Al-MCM adsorption system (i).

impact of the studied chemical anions (NO^{-}, SO^{2-}, PO^{3-}, and CO^{2-}) on the efficiency of CH/Al-MCM as adsorbent for As (V) ions (Figure 10(a)). The high competitive effect was detected during the existence of PO^{3-} as well as CO^{2-} chemical anions as compared to both NO^{-} and SO^{2-} anions (Figure 10(a)). This is credited to the physicochemical similarity between them (As (V) and PO^{3-}) and the tendency of the adsorbed phosphate to create strong inner-sphere complexes [8, 34]. The similarity between CO^{2-} anions and As (V) in the chemical molecular structure is the main reason for the detected carbonate competitive effect on the surface of CH/Al-MCM composite [34]. The low competitive effect of the NO^{-} and SO^{2-} anions was assigned to the adsorption of these anions by types of outer-sphere complexes as compared to the As (V) ions that are commonly adsorbed by stable inner-sphere complexes (Figure 10(a)) [34, 45].

Regarding the actual impacts of Cd (II), Pb (II), Ni (II), and Co (II) cations, they are of strong side and competitive effects on the affinity of the composite for the arsenic ions

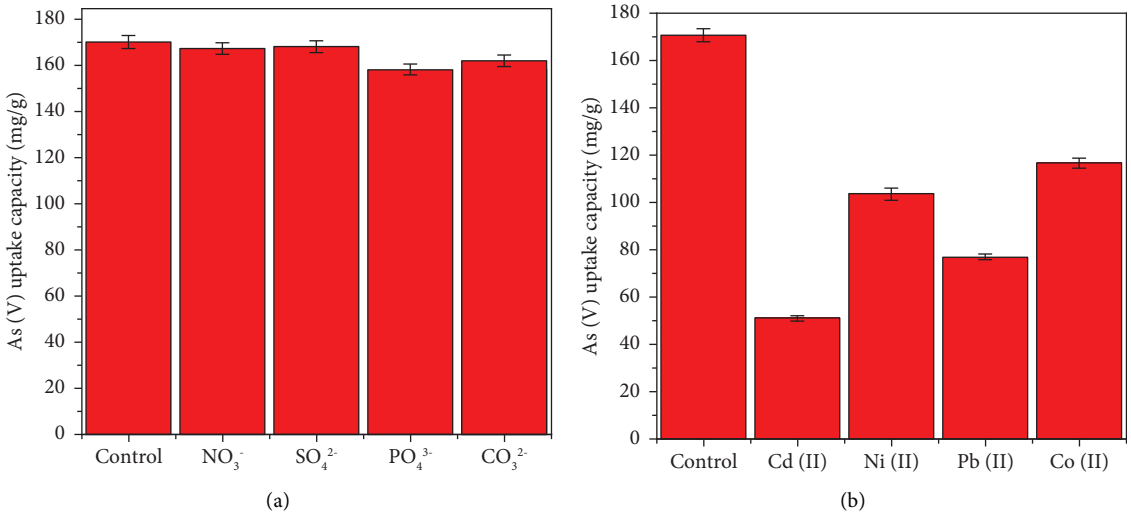

Figure 10: The competitive effects of the other dissolved chemical anions (a) and metal cations (b) on the experimental uptake of As (V) by CH/Al-MCM composite.

(Figure 10(b)). The determined As (V) adsorption capacity declined significantly to 50.8 mg/g, 103.4 mg/g, 76.8 mg/g, and 116.5 mg/g during the coexistence of Cd (II), Ni (II), Pb (II), and Co (II) within the adsorption system (Figure 10(b)). However, the coexisting of such metal ions are of significant adverse impact, the recognized As (V) adsorption results qualify the prepared CH/Al-MCM composite to be applied to realistic remediation of the water resources considering the tested concentrations of the metals.

3.2.5. Influence of the Dosage. The experimental effect of CH/Al-MCM dosage on the actual removal of As (V) was followed from 0.1 g/L to 0.5 g/L. The experimental variables were adjusted at 24 h as equilibrium time, 100 mg/L as the tested concentration, 200 mL as the studied volume, 20°C as temperature, and pH 6. The determined As (V) in the treated samples by different dosages of CH/Al-MCM declared a strong increase in its removal percentages with the regular increase in the solid dosages from 0.1 g/L (12.7%) to 0.7 g/L (100%) (Figure 11). This enhancement impact demonstrates an increase in the surface area of CH/Al-MCM at the water interface as well as the quantities of the reactive sites [21].

3.2.6. Recyclability. The recyclability or reusability of CH/Al-MCM particles is a serious factor during the commercial assessment of the product and realistic applications. The spent particles of CH/Al-MCM were washed with 20 mL of dilute alkaline solution (0.05 M NaOH) for 120 min at a fixed temperature of 20°C. After that, the washed particles were rewashed with distilled water four times and each run consumed 10 min to avoid the effect of the excess NaOH and then dried overnight at 60°C. The previous washing steps were repeated after each reusability test. The experimental variables were adjusted at 24 h as equilibrium time, 400 mg/L as the tested concentration, 200 mL as the studied volume, 0.1 g/L as the used CH/Al-MCM dosage, and 20°C as

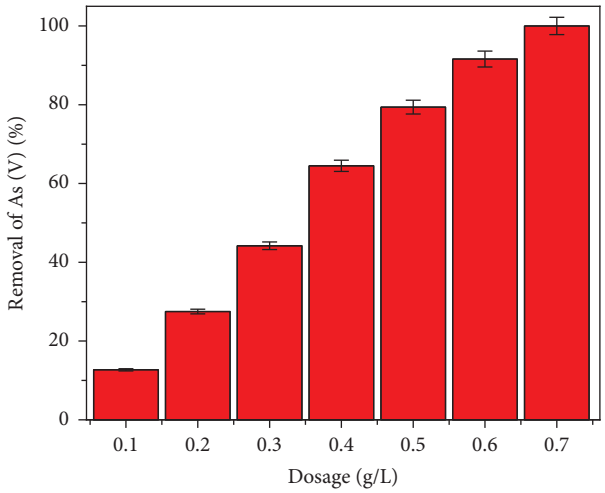

Figure 11: The changes in the As (V) removal percentages as function of the applied CH/Al-MCM dosage.

temperature, and pH 6. The prepared CH/Al-MCM adsorbent exhibits remarkable recyclability and stability considering the number of the investigated cycles as well as the studied concentration (Figure 12). The measured As (V) adsorption capacities by CH/Al-MCM for the investigated six recyclability cycles are 170.4 mg/g (Cycle 1), 169.6 mg/g (Cycle 2), 166.3 mg/g (Cycle 3), 160.4 mg/g (Cycle 4), 152.2 mg/g (Cycle 5), and 143.3 mg/g (Cycle 6) (Figure 12). The observed slight diminution in the measured As (V) uptake capacity by CH/Al-MCM with repeating the recyclability cycles might be assigned to the expected and regular increment in the created chemical complexes between the sequestrated metal ions and the reactive functional groups.

3.2.7. Comparison Study. The determined Q_{sat} values of As (V) by the synthetic structures were assessed in comparison with the other investigated materials in previous studies (Table 2). The structures exhibit higher capacities than most

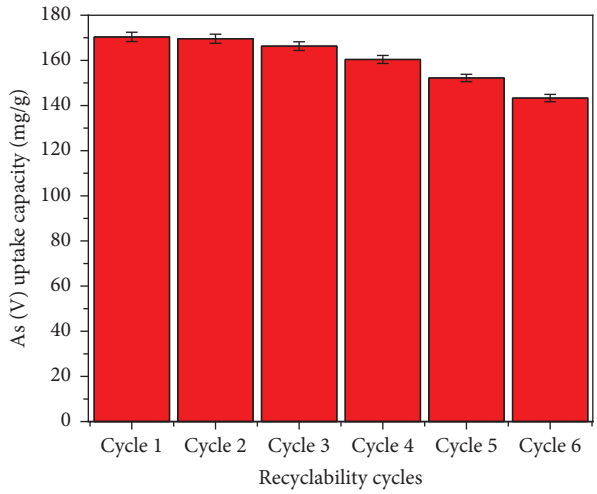

Figure 12: The adsorption efficiency of As (V) during the reusability studies of CH/Al-MCM composite.

Table 2: The determined Q_{sat} values of As (V) by the synthetic structures in comparison with the other investigated materials in previous studies.

Adsorbent	$Q_{(max)}$ (mg/g)	Reference
Goethite/goethite P	34.1	[16]
ZnO/AlSBA-15	123.9	[13]
MWCNTs OCH_2CO_2H	250	[15]
$ZrO(OH)_2$/CNTs	124.5	[46]
0.26_{γ}-Fe_2O_3/SBA−15	23	[47]
Chitosan-coated biosorbent	96.4	[48]
FeOx-GO	113	[49]
MWCNTs	200	[15]
Fe-MWCNTs	250	[50]
GONRs	155.6	[51]
Zirconium-nanoscale carbon	110	[52]
Iron oxide nanoparticle	22.9	[53]
GO/$CuFe_2O_4$ foam	124.6	[54]
Silica-sand/cationized-starch	76.6	[55]
Al-MCM	124	This study
CH/Al-MCM	178.6	This study

of the presented adsorbents, especially for the composite (CH/Al-MCM) (Table 2). This validates the high technical and commercial values of the presented hybrid structure as it was produced from natural raw materials by simplistic synthesis steps in addition to its remarkable safety and environmental value. Therefore, the addressed CH/Al-MCM structure can be escalated to be used effectually in realistic and actual removal of As (V) from industrial wastewater and drinking water.

4. Conclusion

Chitosan/Al-MCM-48 (CH/Al-MCM) was produced by a simple synthesis method as an enhanced and ecofriendly adsorbent structure of the dissolved As (V) ions in the aqueous ecosystem. It achieved As (V) adsorption capacity of 178.6 mg/g which has enhanced values as compared to Al-MCM-41 (124 mg/g). These uptake reactions exhibit the pseudo-first-order kinetic behaviors and classic Langmuir isotherm properties. The theoretically estimated steric parameters reflect a significant enhancement in the density values of the active sites after the functionalization step with chitosan (Nm = 88.8 mg/g for CH/Al-MCM and 61.5 mg/g for Al-MCM). Also, the observed values of the estimated n parameter (2.01 up to 2.66) reveals the possible uptake of 2 to 3 As (V) ions per effective site of CH/Al-MCM by types of multi-ionic mechanisms. The determined As (V) adsorption energy (−16.3 to −16.9 kJ/mol) demonstrates the physical uptake of the metal ions (hydrogen bonding (<30 kJ/mol) and dipole bonding forces (2–29 kJ/mol)). The recognized behaviors of entropy and internal energy as well as the free enthalpy declared the adsorption of As (V) by spontaneous and exothermic processes. Moreover, the composite displays promising reusability and As (V) adsorption capacity either as free ions or under the influence of other dissolved ions.

Data Availability

The data used to support the findings of this study are available from the corresponding authors upon reasonable request.

Additional Points

Recommendation. Further studies will be conducted to follow the kinetic and isotherm properties of the structure as adsorbents of some metal ions considering different values of the solutions pH. This will involve the advanced equilibrium modeling and molecular modeling structure.

Conflicts of Interest

The authors declare that they have no conflicts of interest.

Acknowledgments

The authors thank Princess Nourah bint Abdulrahman University, Riyadh, Saudi Arabia (project number PNURSP2023R5) for supporting this research.

Supplementary Materials

Table S1: nonlinear equations of kinetic, classic isotherm, and advanced isotherm models. Figure S1: schematic diagram for the vertical orientation of the adsorbed As (V) ions on the surface of CH/Al-MCM structure. (*Supplementary Materials*)

References

[1] M. R. Abukhadra, M. Mostafa, M. N. B. Jumah et al., "Insight into the adsorption properties of Chitosan/Zeolite-a hybrid structure for effective decontamination of toxic Cd (II) and As (V) ions from the aqueous environments," *Journal of Polymers and the Environment*, pp. 1–13, 2021.

[2] M. A. Salam, M. R. Abukhadra, and M. Mostafa, "Effective decontamination of As(V), Hg(II), and U(VI) toxic ions

from water using novel muscovite/zeolite aluminosilicate composite: adsorption behavior and mechanism," *Environmental Science and Pollution Research*, vol. 27, no. 12, pp. 13247–13260, 2020.

[3] X. Yang, B. Yan, Y. Liu, F. Zhou, D. Li, and Z. Zhang, "Gamma-FeOOH based hierarchically porous zeolite monoliths for As(V) removal: Characterisation, adsorption and response surface methodology," *Microporous and Mesoporous Materials*, vol. 308, Article ID 110518, 2020.

[4] F. Javaheri, Z. Kheshti, S. Ghasemi, and A. Altaee, "Enhancement of Cd2+ removal from aqueous solution by multifunctional mesoporous silica: equilibrium isotherms and kinetics study," *Separation and Purification Technology*, vol. 224, pp. 199–208, 2019.

[5] M. R. AbuKhadra, M. H. Eid, M. A. El-Meligy, M. Sharaf, and A. T. Soliman, "Insight into chitosan/mesoporous silica nanocomposites as eco-friendly adsorbent for enhanced retention of U (VI) and Sr (II) from aqueous solutions and real water," *International Journal of Biological Macromolecules*, vol. 173, pp. 435–444, 2021.

[6] J. L. Alvarez-Cruz and S. E. Garrido-Hoyos, "Effect of the mole ratio of Mn/Fe composites on arsenic (V) adsorption," *Science of The Total Environment*, vol. 668, pp. 47–55, 2019.

[7] G. Tan, Y. Mao, H. Wang, and N. Xu, "A comparative study of arsenic(V), tetracycline and nitrate ions adsorption onto magnetic biochars and activated carbon," *Chemical Engineering Research and Design*, vol. 159, pp. 582–591, 2020.

[8] X. He, F. Deng, T. Shen et al., "Exceptional adsorption of arsenic by zirconium metal-organic frameworks: engineering exploration and mechanism insight," *Journal of Colloid and Interface Science*, vol. 539, pp. 223–234, 2019.

[9] K. Yoon, D. W. Cho, A. Bhatnagar, and H. Song, "Adsorption of As(V) and Ni(II) by Fe-Biochar composite fabricated by co-pyrolysis of orange peel and red mud," *Environmental Research*, vol. 188, Article ID 109809, 2020.

[10] H. Uppal, S. Chawla, A. G. Joshi, D. Haranath, N. Vijayan, and N. Singh, "Facile chemical synthesis and novel application of zinc oxysulfide nanomaterial for instant and superior adsorption of arsenic from water," *Journal of Cleaner Production*, vol. 208, pp. 458–469, 2019.

[11] M. Usman, M. Zarebanadkouki, M. Waseem, I. A. Katsoyiannis, and M. Ernst, "Mathematical modeling of arsenic(V) adsorption onto iron oxyhydroxides in an adsorption-submerged membrane hybrid system," *Journal of Hazardous Materials*, vol. 400, Article ID 123221, 2020.

[12] Y. K. Penke, A. K. Yadav, I. Malik, A. Tyagi, J. Ramkumar, and K. K. Kar, "Insights of arsenic (III/V) adsorption and electrosorption mechanism onto multi synergistic (redox-photo-electrochemical-ROS) aluminum substituted copper ferrite impregnated rGO," *Chemosphere*, vol. 267, Article ID 129246, 2021.

[13] B. N. Mahato, T. Krithiga, and M. Mary Thangam, "Rapid adsorption of As(V) from aqueous solution by ZnO embedded in mesoporous aluminosilicate nanocomposite adsorbent: parameter optimization, kinetic, and isotherms studies," *Surfaces and Interfaces*, vol. 23, Article ID 100636, 2021.

[14] D. Parajuli, R. Ponte, N. Zhang, T. Nakamura, and T. Kawamoto, "Synthesis and characterization of mixed Co-Zn-ZIF for arsenic(V) adsorption," *Inorganica Chimica Acta*, vol. 502, Article ID 119311, 2020.

[15] T. C. Egbosiuba, A. S. Abdulkareem, A. S. Kovo, E. A. Afolabi, J. O. Tijani, and W. D. Roos, "Enhanced adsorption of As(V) and Mn(VII) from industrial wastewater using multi-walled carbon nanotubes and carboxylated multi-walled carbon nanotubes," *Chemosphere*, vol. 254, Article ID 126780, 2020.

[16] K. Ramirez-Muñiz, F. Perez-Rodriguez, and R. Rangel-Mendez, "Adsorption of arsenic onto an environmental friendly goethite-polyacrylamide composite," *Journal of Molecular Liquids*, vol. 264, pp. 253–260, 2018.

[17] Y. Huang, X. Zeng, L. Guo, J. Lan, L. Zhang, and D. Cao, "Heavy metal ion removal of wastewater by zeolite-imidazolate frameworks," *Separation and Purification Technology*, vol. 194, pp. 462–469, 2018.

[18] J. Park, J. Bae, K. Jin, and J. Park, "Carboxylate-functionalized organic nanocrystals for high-capacity uranium sorbents," *Journal of Hazardous Materials*, vol. 371, pp. 243–252, 2019.

[19] Y. Jiang, M. R. Abukhadra, N. M. Refay, M. F. Sharaf, M. A. El-Meligy, and E. M. Awwad, "Synthesis of chitosan/MCM-48 and β-cyclodextrin/MCM-48 composites as bio-adsorbents for environmental removal of Cd2+ ions; kinetic and equilibrium studies," *Reactive and Functional Polymers*, vol. 154, Article ID 104675, 2020.

[20] A. S. Mohamed, M. R. AbuKhadra, E. A. Abdallah, A. M. El-Sherbeeny, and R. K. Mahmoud, "Photocatalytic performance of silica fume based Co3O4/MCM-41 green nanocomposite for instantaneous degradation of Omethoate pesticide under visible light," *Journal of Photochemistry and Photobiology A: Chemistry*, Article ID 112434, 2020.

[21] M. A. Salam, M. R. AbuKhadra, and A. S. Mohamed, "Effective oxidation of methyl parathion pesticide in water over recycled glass based-MCM-41 decorated by green Co3O4 nanoparticles," *Environmental Pollution*, vol. 259, Article ID 113874, 2020.

[22] M. R. Abukhadra, N. M. Refay, A. Nadeem, A. M. El-Sherbeeny, and K. E. Ibrahim, "Insight into the role of integrated carbohydrate polymers (starch, chitosan, and β-cyclodextrin) with mesoporous silica as carriers for ibuprofen drug; equilibrium and pharmacokinetic properties," *International Journal of Biological Macromolecules*, vol. 156, pp. 537–547, 2020.

[23] H. Chen, S. Fu, L. Fu, H. Yang, and D. Chen, "Simple synthesis and characterization of hexagonal and ordered Al–MCM–41 from natural Perlite," *Minerals*, vol. 9, no. 5, p. 264, 2019.

[24] J. Yuan, H. Ma, Z. Luo, X. Ma, and Q. Guo, "Synthesis of KAlSiO4 by hydrothermal processing on Biotite Syenite and Dissolution reaction kinetics," *Minerals*, vol. 11, no. 1, p. 36, 2020.

[25] J. M. Kalita and M. L. Chithambo, "Structural, compositional and thermoluminescence properties of microcline (KAlSi3O8)," *Journal of Luminescence*, vol. 224, Article ID 117320, 2020.

[26] B. Faraji Dizaji, M. Hasani Azerbaijan, N. Sheisi et al., "Synthesis of PLGA/chitosan/zeolites and PLGA/chitosan/metal organic frameworks nanofibers for targeted delivery of Paclitaxel toward prostate cancer cells death," *International Journal of Biological Macromolecules*, vol. 164, pp. 1461–1474, 2020.

[27] M. Servatan, P. Zarrintaj, G. Mahmodi et al., "Zeolites in drug delivery: Progress, challenges and opportunities," *Drug Discovery Today*, vol. 25, no. 4, pp. 642–656, 2020.

[28] A. I. A. Sherlala, A. A. A. Raman, M. M. Bello, and A. Buthiyappan, "Adsorption of arsenic using chitosan magnetic graphene oxide nanocomposite," *Journal of Environmental Management*, vol. 246, pp. 547–556, 2019.

[29] H. S. Kim, S. H. Lee, C. J. Eun, J. Yoo, and Y. S. Seo, "Dispersion of chitosan nanoparticles stable over a wide pH range by adsorption of polyglycerol monostearate," *Nanomaterials and Nanotechnology*, vol. 10, Article ID 184798042091726, 2020.

[30] A. M. Saad, M. R. Abukhadra, S. Abdel-Kader Ahmed et al., "Photocatalytic degradation of malachite green dye using

chitosan supported ZnO and Ce–ZnO nano-flowers under visible light," *Journal of Environmental Management*, vol. 258, Article ID 110043, 2020.

[31] M. R. Abukhadra, N. M. Refay, A. M. El-Sherbeeny, A. M. Mostafa, and M. A. Elmeligy, "Facile synthesis of bentonite/biopolymer composites as low-cost carriers for 5-fluorouracil drug; equilibrium studies and pharmacokinetic behavior," *International Journal of Biological Macromolecules*, vol. 141, pp. 721–731, 2019.

[32] H. Zhang, H. Sun, D. Zhang et al., "Nanoconfinement of Ag nanoparticles inside mesoporous channels of MCM-41 molecule sieve as a regenerable and H2O resistance sorbent for Hg0 removal in natural gas," *Chemical Engineering Journal*, vol. 361, pp. 139–147, 2019.

[33] H. Wu, J. Zheng, and G. Wang, "Catalytic liquefaction of switchgrass in isobutanol/water system for bio-oil development over bifunctional Ni-HPMo/Fe3O4@Al-MCM-41 catalysts," *Renewable Energy*, vol. 141, pp. 96–106, 2019.

[34] Y. Yin, T. Zhou, H. Luo, J. Geng, W. Yu, and Z. Jiang, "Adsorption of arsenic by activated charcoal coated zirconium-manganese nanocomposite: performance and mechanism," *Colloids and Surfaces A: Physicochemical and Engineering Aspects*, vol. 575, pp. 318–328, 2019.

[35] J. Sun, X. Zhang, A. Zhang, and C. Liao, "Preparation of Fe–Co based MOF-74 and its effective adsorption of arsenic from aqueous solution," *Journal of Environmental Sciences*, vol. 80, pp. 197–207, 2019.

[36] M. N. B. Jumah, M. H. Eid, A. A. AL-Huqail et al., "Enhanced remediation of As (V) and Hg (II) ions from aqueous environments using β-cyclodextrin/MCM-48 composite: batch and column studies," *Journal of Water Process Engineering*, vol. 42, Article ID 102118, 2021.

[37] Y. Huang, S. Li, J. Chen, X. Zhang, and Y. Chen, "Adsorption of Pb(II) on mesoporous activated carbons fabricated from water hyacinth using H3PO4 activation: adsorption capacity, kinetic and isotherm studies," *Applied Surface Science*, vol. 293, pp. 160–168, 2014.

[38] P. Li, B. Gao, A. Li, and H. Yang, "Highly selective adsorption of dyes and arsenate from their aqueous mixtures using a silica-sand/cationized-starch composite," *Microporous and Mesoporous Materials*, vol. 263, pp. 210–219, 2018.

[39] H. M. El-Zeiny, M. R. Abukhadra, O. M. Sayed, A. H. Osman, and S. A. Ahmed, "Insight into novel β-cyclodextrin-grafted-poly (N-vinylcaprolactam) nanogel structures as advanced carriers for 5-fluorouracil: equilibrium behavior and pharmacokinetic modeling," *Colloids and Surfaces A, Physicochemical and Engineering Aspects*, vol. 586, Article ID 124197, 2020.

[40] L. Sellaoui, H. Guedidi, S. SarraWjihi et al., "Experimental and theoretical studies of adsorption of ibuprofen on raw and two chemically modified activated carbons: new physicochemical interpretations," *RSC Advances*, vol. 6, no. 15, pp. 12363–12373, 2016.

[41] F. Dhaouadi, L. Sellaoui, M. Badawi et al., "Statistical physics interpretation of the adsorption mechanism of Pb2+, Cd2+ and Ni2+ on chicken feathers," *Journal of Molecular Liquids*, vol. 319, Article ID 114168, 2020.

[42] L. Sellaoui, J. Ali, M. Badawi, A. Bonilla-Petriciolet, and Z. Chen, "Understanding the adsorption mechanism of Ag+ and Hg2+ on functionalized layered double hydroxide via statistical physics modeling," *Applied Clay Science*, vol. 198, Article ID 105828, 2020.

[43] M. Mobarak, R. A. Ali, and M. K. Seliem, "Chitosan/activated coal composite as an effective adsorbent for Mn(VII): modeling and interpretation of physicochemical parameters," *International Journal of Biological Macromolecules*, vol. 186, pp. 750–758, 2021.

[44] F. Dhaouadi, L. Sellaoui, H. E. Reynel-Ávila et al., "Adsorption mechanism of Zn2+, Ni2+, Cd2+, and Cu2+ ions by carbon-based adsorbents: interpretation of the adsorption isotherms via physical modelling," *Environmental Science & Pollution Research*, vol. 28, no. 24, pp. 30943–30954, 2021.

[45] M. Dutta, D. Agarwal, M. Sivakami, A. K. Gupta, and M. K. Yadav, "Hollow polyaniline microsphere/Fe_3O_4 nanocomposite as an effective adsorbent for removal of arsenic from water," *Indian journal of medical ethics*, vol. 5, no. 4, pp. 1–14, 2020.

[46] D. Liu, S. Deng, A. Maimaiti et al., "As(III) and As(V) adsorption on nanocomposite of hydrated zirconium oxide coated carbon nanotubes," *Journal of Colloid and Interface Science*, vol. 511, pp. 277–284, 2018.

[47] X. Peng, Y. Zhao, T. Yang et al., "One-step and acid free synthesis of γ-Fe 2 O 3/SBA-15 for enhanced arsenic removal," *Microporous and Mesoporous Materials*, vol. 258, pp. 26–32, 2018.

[48] V. M. Boddu, K. Abburi, J. L. Talbott, E. D. Smith, and R. Haasch, "Removal of arsenic (III) and arsenic (V) from aqueous medium using chitosan-coated biosorbent," *Water Research*, vol. 42, no. 3, pp. 633–642, 2008.

[49] H. Su, Z. Ye, and N. Hmidi, "High-performance iron oxide–graphene oxide nanocomposite adsorbents for arsenic removal," *Colloids and Surfaces A: Physicochemical and Engineering Aspects*, vol. 522, pp. 161–172, 2017.

[50] H. Alijani and Z. Shariatinia, "Effective aqueous arsenic removal using zero valent iron doped MWCNT synthesized by in situ CVD method using natural α-Fe2O3 as a precursor," *Chemosphere*, vol. 171, pp. 502–511, 2017.

[51] M. H. Sadeghi, M. A. Tofighy, and T. Mohammadi, "One-dimensional graphene for efficient aqueous heavy metal adsorption: rapid removal of arsenic and mercury ions by graphene oxide nanoribbons (GONRs)," *Chemosphere*, vol. 253, Article ID 126647, 2020.

[52] N. Mahanta and J. P. Chen, "A novel route to the engineering of zirconium immobilized nano-scale carbon for arsenate removal from water," *Journal of Materials Chemistry A*.vol. 1, no. 30, pp. 8636–8644, 2013.

[53] C. G. Lee, P. J. Alvarez, A. Nam et al., "Arsenic(V) removal using an amine-doped acrylic ion exchange fiber: kinetic, equilibrium, and regeneration studies," *Journal of Hazardous Materials*, vol. 325, pp. 223–229, 2017.

[54] L. K. Wu, H. Wu, Z. Z. Liu et al., "Highly porous copper ferrite foam: a promising adsorbent for efficient removal of As(III) and As(V) from water," *Journal of Hazardous Materials*, vol. 347, pp. 15–24, 2018.

[55] Z. Li, L. Wang, J. Meng et al., "Zeolite-supported nanoscale zero-valent iron: new findings on simultaneous adsorption of Cd(II), Pb(II), and As(III) in aqueous solution and soil," *Journal of Hazardous Materials*, vol. 344, pp. 1–11, 2018.